IEEE Access
Multidisciplinary | Rapid Review | Open Access Journal

Received 18 October 2022, accepted 27 November 2022, date of publication 6 December 2022, date of current version 21 December 2022.

Digital Object Identifier 10.1109/ACCESS.2022.3227107

RESEARCH ARTICLE

Realistic Human Exposure at 3.5 GHz and 28 GHz for Distributed and Collocated MaMIMO in Indoor Environments Using Hybrid Ray-Tracing and FDTD

ROBIN WYDAEGHE, SERGEI SHIKHANTSOV, EMMERIC TANGHE, (Member, IEEE), GÜNTER VERMEEREN, (Member, IEEE), LUC MARTENS, (Member, IEEE), PIET DEMEESTER, (Fellow, IEEE), AND WOUT JOSEPH, (Senior Member, IEEE)
Department of Information Technology, Ghent University/IMEC, 9052 Ghent, Belgium

Corresponding author: Robin Wydaeghe (Robin.Wydaeghe@UGent.be)

This work was supported in part by the European Research Council (ERC) through ATTO: A New Concept for Ultrahigh Capacity Wireless Networks under Grant 695495 and in part by Methusalem through SHAPE: Next Generation Wireless Networks.

ABSTRACT Realistic human downlink exposure at 3.5 and 28 GHz to electromagnetic fields is evaluated for distributed and collocated base stations using a hybrid ray-tracing/finite-difference time-domain method. For the first time, the absorbed power density is computed for distributed massive multiple-input multiple-output (DMaMIMO) 6G base stations at 28 GHz. The results are compared with 3.5 GHz 5G base stations. Computational costs are drastically increased at 28 GHz. A large analysis is realized by speed improvements and using two configurations. In the first, exposure distributions of DMaMIMO BS show *clusters* of low and high exposure. These clusters disappear when results are normalized with respect to the incoming power at the user. In the second, the influence of BS to user distance in line-of-sight (LOS) and non-line-of-sight (NLOS) scenarios shows expected results. This includes a power law relationship in LOS and shadowing in NLOS. The vast majority of exposure quantities are less than 4% of the limits of the International Commission for Non-Ionizing Radiation. Basic restrictions are respected when reference quantities are set to their limits. With equal power, distributed base stations contribute 2 to 3 times less to exposure than collocated base stations. Expressed as a ratio to their limits set by ICNIRP, the basic quantities are 5 to 10 dB lower than the reference quantities.

INDEX TERMS 5G, 6G, DMaMIMO, mm-Waves, ray-tracing, FDTD, EMF-exposure, absorbed power density.

I. INTRODUCTION

The demand for more performant wireless networks is continuously increasing. Applications such as autonomous vehicles, Internet of Things (IoT) and Industry 4.0 require extremely reliable, ultra-low latency and very high throughput wireless connectivity [1]. The fifth generation (5G) of cellular networks has addressed these needs with a number of solutions [2], [3]. One such technology is Massive Multiple-Input-Multiple-Output (MaMIMO) [4]: a large number of antennas in the transmitter (Tx) enables precoding (or *beamforming* [5]) to exploit the environment's spatial diversity, thereby increasing the network capacity [6]. Commercial MaMIMO deployment is ongoing [7, Sec. 5], [8]. This has prompted the research literature to focus on the question "*What is next?*", proposing *Distributed* MaMIMO proposed as a prospective sixth generation (6G) technology [9]. A MaMIMO base station (BS) is *distributed* (DMaMIMO) when its antenna elements are located in different geographic positions [10], i.e., the separation is much larger

The associate editor coordinating the review of this manuscript and approving it for publication was Hassan Tariq Chattha.

than the wavelength. When the separation is electrically small, channel capacity is hindered by *unfavorable propagation conditions* (reduced "mutual orthogonality among the vector-valued channels to the terminals" [11]) and *pilot contamination* [12]. When the separation is electrically large, the channel orthogonality increases with antenna density [13]. Also, the broader paradigm envisions a *cell-free* MaMIMO network of Access Points (AP), effectively removing pilot contamination [13], [14]. Another way 5G delivers on its ultra-low latency and exceptional data throughput is by increasing the operating frequency. The first frequency band (FR1) around 3.5 GHz is employed by the majority of commercially sold 5G BSs in Europe. The second frequency band (FR2) around 28 GHz is also known as the *mm-Wave* 5G band. In ideal conditions, the larger bandwidths enables record-breaking data rates [15], [16]. However, the higher free-space path loss limits the use of mm-Waves to short UE-to-BS distance, such as near an AP. Therefore, DMaMIMO and high mm-Waves frequencies are two 6G directions that work constructively.

The assessment of human exposure to electromagnetic fields (EMFs) is of great importance for public health [17]. The International Commission on Non-Ionizing Radiation Protection (ICNIRP) provides internationally accepted safety guidelines that limit certain exposure metrics [18]. While worst-case exposure has been the subject of much research guaranteeing safety [19], [20], less is known about *realistic* exposure. To achieve this, the propagation and exposure steps need to be rigorously integrated into one method, for example by hybridizing ray tracing (RT) with the finite-difference time-domain (FDTD) method [21] or a spherical near-field transformation with FDTD [23]. Recently, the influence of DMaMIMO on the behavior of *hotspots* and their resulting exposure has been examined at 3.5 GHz [24]. The latest update of the ICNIRP guidelines in 2020 [18] introduces the absorbed power density S_{ab} in the basic restriction above 6 GHz. The extension of realistic exposure of DMaMIMO BSs at 28 GHz is, to the best knowledge of the authors, an open question. This paper is first to provide answers in this unexplored research domain. The main novelty is proposing for the first time the hybrid RT/FDTD method at mm-Wave frequencies. Furthermore, the use of realistic state-of-the-art BSs is considered here. These enable two important novel results. In a realistic exposure scenario at 28 GHz, we present the first

1) comparison between distributed and collocated MaMIMO BS exposure;
2) quantification of the new basic quantity S_{ab} for new MaMIMO technologies.

We also provide the first comparison between these results at 3.5 GHz and 28 GHz.

II. METHODS

A. CONFIGURATIONS

Figures 1a and 1b each show a realization of the two industrial environments studied. In both, a closed concrete ($\varepsilon_r = 7$, $\sigma = 1.5 \times 10^{-2}$ S/m) room containing metal cuboids models a Factory of the Future (FotF). The cuboids have a fixed footprint and variable height as in [21], and model, e.g., metal machinery. Their position is sampled from two spatial distributions covering the room, detailed below. These scatterers reflect and diffract the EMFs transmitted by the BS's antenna elements, which aims to replicate the propagation diversity of a realistic indoor environment. This collocated or distributed MaMIMO BS models a 5G BS or extremely large aperture array (ELAA), respectively. An array of patch antennas is suspended 1 and 2 m from the ceiling in configuration 1 and 2, respectively. They emit a signal at 3.5 GHz or 28 GHz (mm-Waves). This is shown in blue in Fig. 1. Isotropic receiver antennas (Rxs) receive this signal. Their height is 1.75 m, their polarization is vertical and their positions are on a straight line parallel to the room's walls. They model the user equipment (UE) held next to the head of humans (shown in red) walking in the FotF. Two pairs of channel types (*configurations*) are studied, namely (i) collocated and distributed MaMIMO channels and (ii) LOS and NLOS channels.

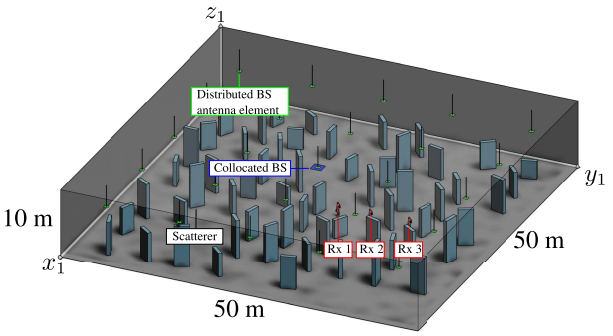

(a) The first configuration, comparing collocated with distributed MaMIMO BSs. The first BS is located at the center of the room. The second has its elements spread over the room.

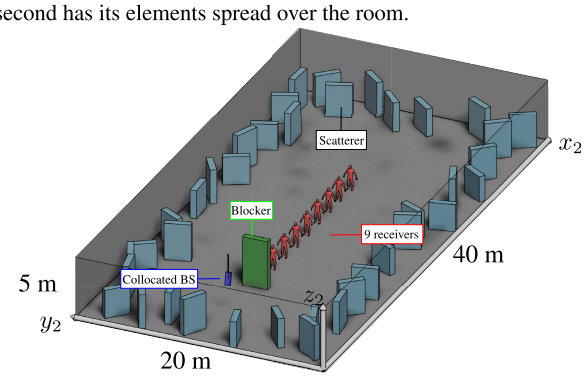

(b) The second configuration, comparing LOS with NLOS exposure. The NLOS blocker shown here in green is removed for the LOS case.

FIGURE 1. Two indoor industrial environments studied. Shown here are examples of realizations with randomly selected scatterers. The Rxs in red merely indicate their position and do not scatter any rays. Some walls and the ceiling are shown transparent for clarity in this figure.

1) COLLOCATED (COL) AND DISTRIBUTED MaMIMO (DIS) CHANNELS

The room's footprint is square and has dimensions $50 \times 50 \times 10$ m^3. The distribution of the scatterers is as in [24],

i.e., by removing randomly 30% of the scatterers on a uniform grid.

Three UEs receive a signal. The number of Rxs is chosen low to reduce computational costs. The number of channel realizations is chosen high (100) to enable a statistical analysis of the exposure distributions. The first UE is placed at a horizontal separation from the BS (henceforth UE separation) of 2.5 m. The second and third have a UE separation of 7.5 and 12.5 m.

2) LINE-OF-SIGHT (LOS) AND NON-LINE-OF-SIGHT (NLOS) CHANNELS

The room's footprint is rectangular with dimensions $40 \times 20 \times 5$ m^3. The distribution of the scatterers is as in [21], i.e., using the Poisson Disk sampling algorithm. Results are given with and without a $2 \times 0.5 \times 5$ m^3 blocker. Nine UEs receive a signal to enable an analysis as function of receiver position. The first and last Rx have a UE separation of 6 and 22 m, respectively. The number of channel realizations is chosen low (5) to reduce computational costs.

3) PARAMETERS

The n77 and n261 frequency bands are used throughout the numerical pipeline. In the following, we refer to these as the 3.5 and 28 GHz bands, respectively. Their spectrum parameters are listed in Table 1. Two realistic BSs are modeled for 5G coverage at these frequencies. Their physical parameters are listed in Table 3.

TABLE 1. Spectrum parameters of the 3.5 and 28 GHz bands employed in the simulations.

	3.5 GHz band	28 GHz band
Frequency band	n77	n261
Central frequency [GHz]	3.75	27.9
Wavelength [mm]	0.0799	0.0107

The parameters used for the RT simulations are shown in Table 2. These parameters are sufficient to accurately predict the channel in the modeled indoor environment [22]. The MaMIMO BS is an array consisting of equally spaced dual-polarized antenna elements. Their parameters are also listed in Table 3. The inter-element spacing in the collocated MaMIMO BS is 0.5λ for both the vertical and horizontal direction. In the distributed case, the inter-element spacing is 10 m, such that it covers the whole room.

B. RT-FDTD

The hybrid RT-FDTD tool developed in [21] is extended to mm-Wave frequencies. The fundamental method is the same: the scattered EMFs by plane waves (PWs) are first stored and then combined based on the full channel matrix. The schematic specifies how this fundamental method is looped over all parameters of interest, for one configuration. The RT and FDTD initialization followed by their hybridization are detailed schematically in Fig. 2.

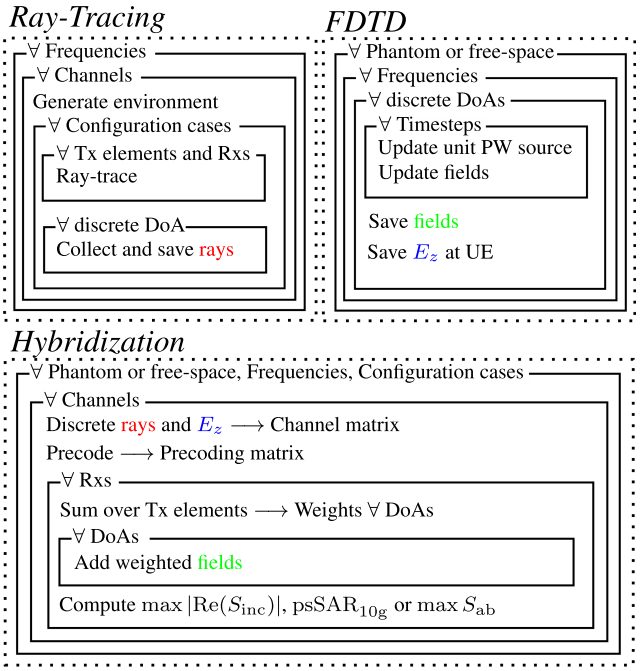

FIGURE 2. Schematic detailing the full numerical pipeline for a configuration. The initialization consists of independent RT and FDTD parts. Using the colored data, the hybridization step yields exposure quantities. A labeled box indicates its contents are looped over the dimension denoted by the for all symbol ∀. *Configuration cases* refer to DIS/COL or LOS/NLOS in configuration 1 and 2, respectively.

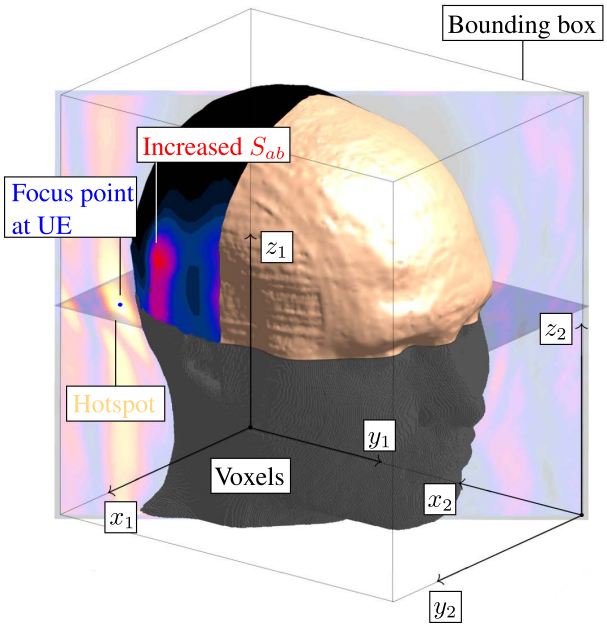

FIGURE 3. FDTD-domain. A hotspot is shown in yellow around the focus point in blue. Increased surface absorbed power density S_{ab} is shown in red on the skin. The phantom including the skin, shown in beige, is voxelized at 28 GHz, shown in grey.

For the FDTD initialization and exposure evaluation, a number of adaptations are made. These are shown visually in Fig. 3. A Multimodal Imaging-Based Detailed Anatomical

TABLE 2. Computational parameters of the ray-tracing simulations for both configurations and both frequency bands.

	Configuration 1: COL/DIS		Configuration 2: LOS/NLOS	
	3.5 GHz band	28 GHz band	3.5 GHz band	28 GHz band
Reflections	5	5	6	5
Transmissions	0	0	2	2
Diffractions	1	1	2	1
Threshold [dBm]	-250			
Angular spacing [°]	0.25			
Collection radius [cm]	31.5		20.0	

TABLE 3. Physical parameters of the realistic BSs for both configurations and both frequency bands. The Ericsson BSs parameters are not publicly available and are therefore informed estimations based on, among others, the size of the device.

	Configuration 1: COL/DIS		Configuration 2: LOS/NLOS	
	3.5 GHz band	28 GHz band	3.5 GHz band	28 GHz band
Base station model name	N/A	N/A	Ericsson AIR 6449	Ericsson StreetMacro 6701
Total EIRP power[a] [dBm]	55			
Antenna configuration[b]	$1 \times 5 \times 5$	$1 \times 5 \times 5$	$2 \times 8 \times 12$	$2 \times 8 \times 8$
Inter-element spacing [λ]	COL: $0.5\lambda \times 0.5\lambda$ DIS: $10\,\text{m} \times 10\,\text{m}$		0.89×0.71	6.8×2.7
Antenna element type	Patch antenna (ε_r=4.4)	Patch antenna (ε_r=4.4)	Dipole (PEC)	Dipole (PEC)
Element dimensions [mm]	$3 \times 3 \times 1.5$	$3 \times 3 \times 1.5$	$79.9 \times 0 \times 0$	$10.7 \times 0 \times 0$
Maximum gain[c] [dBi]	4.79	7.35	2.15	2.15
Tilt [°]	90 (facing the floor)		10 (facing the Rx)	

[a]The total EIRP power is fed equally among the antenna elements.
[b]The first dimension corresponds to the number of polarizations. When equal to two, the bowtie formation is used.
[c]The maximum gain is the gain normal to the antenna element array plane.

Model of the Human Head and Neck (MIDA) [25] is used as a phantom. The phantom is highly detailed and features a spatial isotropic resolution of 500 µm [26], shown in the upper front head. The model is finely voxelized due the small wavelength used, shown in the lower head. The head faces the BS, i.e., in the positive y_1-direction or negative x_2-direction for configuration 1 and 2, respectively. Maximum ratio transmission (MRT) precoding is used in a single-user down-link (DL) transmission scenario. The incoming rays focus the z-component of the electric field to the location of a vertical dipole, representing the UE. A vertical and horizontal slice of the domain indicates by means of yellow and white colors that the volume around the focus point contains increased EMFs compared to the background. This *hotspot* is a result of focused rays interfering constructively. The focus point is located 2 cm behind the right ear, within the bounding box of the phantom. This location results in a worst-case exposure scenario because the most common region of maximum exposure is the skin of the ears [24]. The surface absorbed power density S_{ab} averaged over a 4-cm^2 surface is shown on the back of the head. The indicated red colors reveal a region near the hotspot where it is increased.

C. COMPUTATIONAL CONSIDERATIONS

The MaMIMO BS requires the knowledge of the wireless channel to perform the precoding. We calculate the channel matrix coefficient as the sum of the signals with different directions of arrival (DoAs) [27]. A signal is the electric field's z-component received at the location of the UE. The field is computed with an FDTD simulation of a unit PW incident on the human head phantom.

The higher frequency results in prohibitively large computational costs (due to, e.g., the Courant limit [28]). Therefore, the execution time of each FDTD simulation at 28 GHz is reduced by a combination of techniques. First, the workflow of Fig. 2, including pre- and post-processing, is parallelized on a high-performance computing cluster with 40 CPUs and a performant GPU. Second, the ray approximation is more justified at higher frequencies, reducing the number of required rays in the RT simulations. As a result, the number of reflections and diffractions is decreased, as shown in Table 2. Finally, at 27.9 GHz the millimeter-sized voxels overresolve the model's head features. This gives us the freedom to reduce the voxel size to $\lambda/14 = 1.75\,\text{mm}$. This is not the case for 3.75 GHz, where the voxel size must be at least $1.75\,\text{mm} = \lambda/46$. The number of voxels at 3.5 and 28 GHz is 1.54 and 22.12 million, respectively. However, the computing and memory costs remain high. More importantly, the substantially increased memory load of the electromagnetic field data restricts the number of DoAs, channel realizations, and UE separations because, for each of these, the data is exported, added and weighted. Therefore, the number of FDTD simulations must be reduced. The number of DoAs is set to 20, which still enables the modeling of hotspots. The error is estimated in [21].

In configuration 1, the number of channel realizations is chosen large (100). Therefore, we study the exposure distributions in this configuration. In configuration 2, the number of receivers is chosen large (9). Thus, we study the influence of position in this configuration.

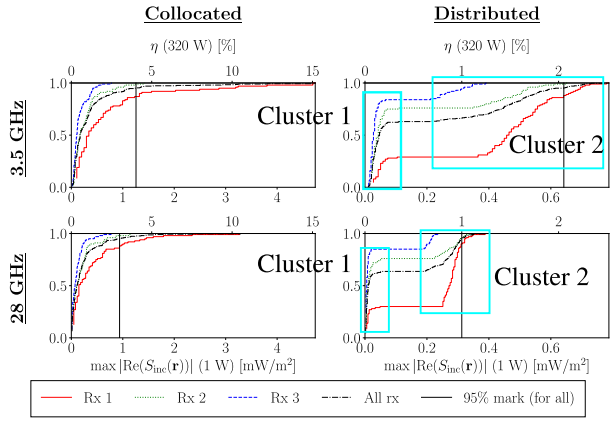

FIGURE 4. Reference quantities normalized for a 1 W radiating BS in configuration 1. Clarification of this figure is provided in Section III-A. In the distributed MaMIMO case, two exposure clusters can be seen, delimited around $0.19\,\mathrm{mW/m^2}$, shown in cyan on the horizontal axis.

D. EXPOSURE ASSESSMENT

The reference levels defined by the ICNIRP for human exposure at both 3.5 and 28 GHz is the power flux density S_{inc} in free-space. Here, a free-space computational domain is simulated without phantom. The MIDA phantom is added when simulating for the basic restrictions. The basic restriction at 3.5 GHz is given by the peak-spatial specific absorption rate averaged over a 10-g cube ($\mathrm{psSAR_{10g}}$ in W/kg) [18], [29]. At 28 GHz, the maximum surface absorbed power density S_{ab} (in $\mathrm{W/m^2}$) averaged over a 4-$\mathrm{cm^2}$ surface is used to better account for the superficial nature of the exposure [18], [30]. We define η as the percentual ratio between each simulated exposure quantity γ ($|\mathrm{Re}S_{\mathrm{inc}}|$, $\mathrm{psSAR_{10g}}$ or S_{ab}) and its maximum allowed value for the general public (GP) γ_{limit}, as set by the ICNIRP guidelines:

$$\eta_\gamma = \frac{\gamma}{\gamma_{\mathrm{limit}}} \cdot 100\% \,. \tag{1}$$

The values of γ_{limit} are listed in Table 4. Note that all exposure quantities are local to the head and time-averaged. When the reference quantity (S_{inc}) is set to the reference level ($10\,\mathrm{W/m^2}$), the basic quantities ($\mathrm{psSAR_{10g}}$ and S_{ab}) should be below their exposure limit. Dividing these by η_{r} is equivalent to setting the reference quantities to the reference levels. This results in the definition of α,

$$\alpha = \frac{\eta_{\mathrm{b}}}{\eta_{\mathrm{r}}} \cdot 100\% \,, \tag{2}$$

where η_{b} is the η of the basic restrictions. A value of α above 100% means that the basic restrictions would be exceeded if incident power densities are set to the reference levels. This is called hotspot normalization [31].

III. RESULTS

A. GENERAL RESULTS

In Figures 4 through 7, results from the first configuration (COL/DIS) are presented in a matrix of plots, comparing across frequency (the 3.5 and 28 GHz frequency bands) and BS type (the collocated and distributed MaMIMO BSs). The main interest is how the exposure values are distributed for each of these cases. The vertical axes reads the Cumulative Distribution Functions (CDFs) of the exposure quantity from the 100 channel realizations. The bottom horizontal axes of the plots are the normalized exposure quantities. The top horizontal axes is scaled such that it displays the corresponding η value for the actual output power of 320 W (55 dBm). Three colored lines are associated with each Rx shown in Fig. 1a. The "*All rx*" line combines all 300 channel realizations into one CDF. A vertical line denotes the quantity that is greater than 95% of all these realizations' quantities.

TABLE 4. Exposure quantities γ and their limiting values in both frequency bands according to the ICNIRP 2020 guidelines for the general public. The quantities are averaged over space and time as defined in the text.

$\gamma \leq \gamma_{\mathrm{limit}}$	3.5 GHz band	28 GHz band
Reference level	$\lvert\mathrm{Re}\,S_{\mathrm{inc}}\rvert \leq 10\,\mathrm{W/m^2}$	$\lvert\mathrm{Re}\,S_{\mathrm{inc}}\rvert \leq 10\,\mathrm{W/m^2}$
Basic restriction	$\mathrm{psSAR_{10g}} \leq 2\,\mathrm{W/kg}$	$S_{\mathrm{ab}} \leq 20\,\mathrm{W/m^2}$

In Fig. 8 and 9, results from the second configuration compare the 3.5 and 28 GHz bands side by side. The main interest is how the exposure values depend on position to the BS and presence of a blocker. The left and right vertical axis indicates the relevant exposure quantity and its corresponding η value at 320 W BS output power. The horizontal axis reads the UE separation. Two lines are associated with the absence (LOS) or presence (NLOS, shown in Fig. 1b) of the blocker. Each result is represented by a dot. The number of channel realizations is 5, which estimates the mean and standard deviation of the exposure in LOS or NLOS. Lines connect the average of the 5 channel realizations across UE separation.

B. CONFIGURATION 1: COL VS DIS

In general, the Rxs closest to the BS have the highest exposure, in particular for the first Rx. However, the focus of this configuration's analysis is not on position, but on the distributions of exposure quantities. One hundred channel realizations were necessary to sufficiently resolve the exposure distributions.

1) REFERENCE QUANTITIES

The results of the reference quantities are shown in Figure 4. Realistic values are at most 4% of their limits in 95% of cases for a BS radiating 320 W. All exposure metrics are 2 to 3 times less with a distributed BS compared to a collocated BS. For the distributed BS, more elements are distant from the receivers, reducing the total incoming power. The exposure distribution with the collocated BS can be well modeled by a Ricean fading channel. This suggests that a LOS component or strong reflection path dominates the channel. The distributed BS does not generate a Ricean fading channel. Instead, two regions are identified of low and high exposure (Fig. 4, right), delimited around $0.19\,\mathrm{mW/m^2}$. We call these

exposure clusters. In the first cluster, a similar exposure distribution to the collocated BS is seen. The standard deviation of the second cluster is 4.5 times broader than the first. These results can be explained as follows. When a UE is surrounded by scatterers, the probability that exposure belongs to the first cluster is highest. The channel resembles that of the collocated BS, because the interaction happens mainly by one or a few nearby antenna elements. When no nearby scatterers shadow the UE, the probability that exposure belongs to the second cluster is highest. The interaction can now occur with a larger number of antenna elements farther from the UE. Therefore, the number of reflections and diffractions taken by the rays is higher. The variability in exposure is thus higher. As seen in Fig. 1a, the scatterers belong to a regular grid, the antenna elements are directly above this grid, and the receivers are located at the center of each grid cell. This set-up makes it possible for receivers to be completely encircled or not by scatterers. Similar exposure distributions are observed when comparing the 3.5 and 28 GHz bands. With the collocated BS, the 95$^{\text{th}}$ percentile is 12% lower at mm-Wave frequencies. With the distributed BS, the reduction is 55%. In this case, the standard deviation of the second exposure cluster is much lower. This is likely due to the increased path loss at these frequencies reducing the number of interactions with distant antenna elements.

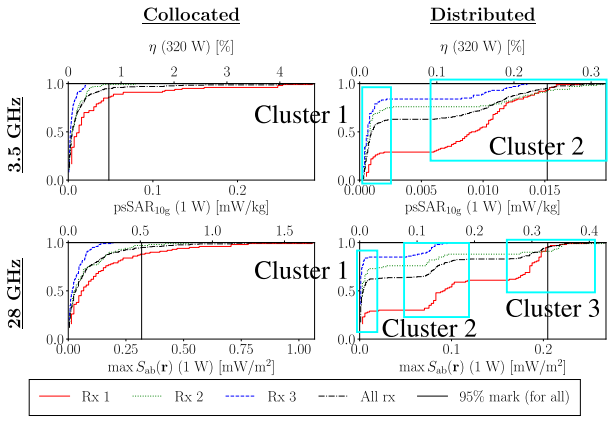

FIGURE 5. Basic quantities normalized for a 1 W radiating BS in configuration 1. Clarification of this figure is provided in Section III-A. In the distributed MaMIMO case, exposure clusters can be seen, shown in cyan on the horizontal axis. For 28 GHz, three are seen, delimited around $0.05\,\text{mW/m}^2$ and $0.15\,\text{mW/m}^2$.

2) BASIC QUANTITIES

The results of the basic quantities are shown in Fig. 5. Realistic values are at most 0.85% of their limits in 95% of cases. Note that these η values are generally 5 to 10 dB lower compared to those of the reference quantities. As a result, the α value is less than one and the basic quantities stay 5 to 10 dB below their limits when the reference quantities are set to their limits. The same conclusions as above can be drawn about the values and exposure distributions. The incoming electric fields are identical because the propagation of the rays onto the phantom is the same (the *propagation step*). Differences between Fig. 4 and 5 can only be attributed to the exposure metric used and the presence of the phantom (the *exposure step*, shown in Fig. 3). Because similar results are seen, the exposure step is mostly independent of the propagation step. However, in the 28 GHz band with the distributed BS, three exposure clusters are seen, delimited around 0.05 and $0.15\,\text{mW/m}^2$. This deviation can only be explained by the interplay of the propagation and exposure step. Because high exposure clusters are more prominent in NLOS propagation, the formation of hotspots is more likely in the high exposure clusters. When the location of the hotspot is within a certain distance of the skin, the hotspot causes increased exposure. This is registered only by the superficial S_{ab} exposure metric on the phantom's skin. The aforementioned α value is highest in this case because of this effect.

3) NORMALIZED RESULTS TO INCOMING RX POWER

Before the precoding step, the total power is split evenly among the antenna elements. In the distributed MaMIMO BS case, the receiver is surrounded by a small number of antenna elements each having a fraction of the total output power. In the collocated MaMIMO BS case, the receiver is near all antenna elements radiating the total output power. The exposure quantities are therefore substantially lower with distributed BSs compared to collocated ones. Commercial distributed MaMIMO BSs do not exist yet; neither do corresponding regulations. It is therefore unknown what realistic total output powers will be of these systems. The output power is presumably higher, and likely dependent on the number of antenna elements and the area covered. Therefore, the above conclusion may not be realistic due to the equal power assumption. There are a number of ways to *normalize* the exposure quantities such that a fair comparison becomes possible. One of them is dividing the result by the total incoming power P^{Rx} on the Rx. The total electric field is

$$E^{\text{tot}} = \sum_i w_i \hat{E}_i \,,$$

where i denotes a DoA angle, w_i is the corresponding weight from the precoding matrix and $\hat{E}_i$ is the electric field for a unit PW with DoA angle i. The total incoming power is defined as

$$P^{\text{Rx}} = \sum_i |w_i|^2 \,.$$

The results are now normalized w.r.t. both 1 W total power from the Tx and 1 W incoming power on the Rx. The simulated exposure value γ is retrieved as follows:

$$\gamma = P_{\text{BS}} \cdot P^{\text{Rx}} \gamma_{1\,\text{W}}^{1\,\text{W}} \,.$$

In this equation, P_{BS} is the BS's total emitted power and $\gamma_{1\,\text{W}}^{1\,\text{W}}$ is the doubly normalized exposure quantity. The latter is shown in Figures 6 and 7 for the reference and basic quantities, respectively. As the propagation step is effectively removed, there is no statistically significant dependence on

receiver position for the reference quantities. For the basic quantities, there is a pronounced dependence on position in the mm-Wave distributed case. This validates the previous conclusion that a strong skin coupling with the hotspots in the exposure step is present. For Rx 2 and 3, two clusters are seen delimited by approximately 5 μW/m^2. This causes the three clusters observed earlier, which were only present for Rx 2 and 3. In all other cases, exposure distributions are well modeled by a normal distribution.

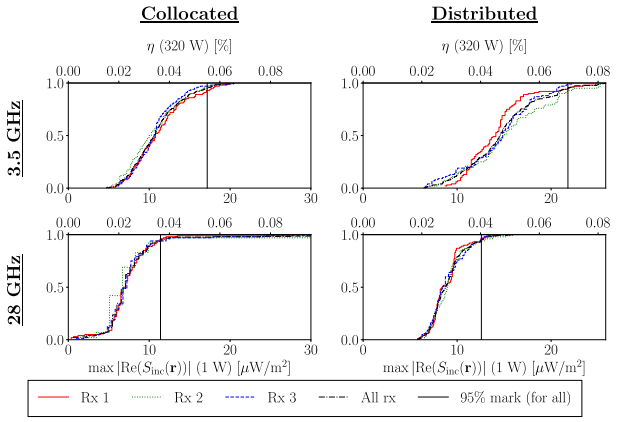

FIGURE 6. Reference quantities normalized for a 1 W radiating BS and for 1 W total incident power on the Rx in configuration 1. Clarification of this figure is provided in Section III-A. No clusters are observed.

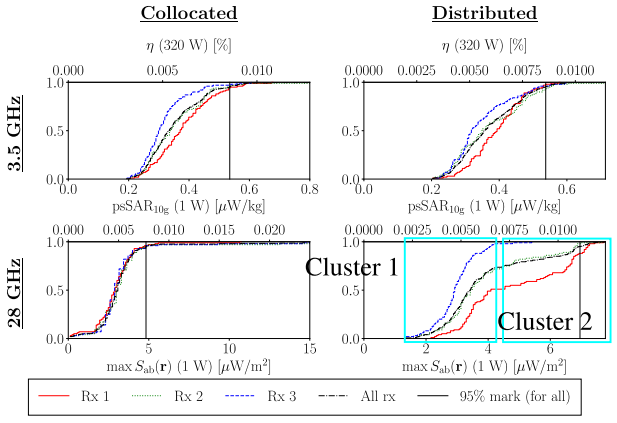

FIGURE 7. Basic quantities normalized for a 1 W radiating BS and for 1 W total incident power on the Rx in configuration 1. Clarification of this figure is provided in Section III-A. Clusters, shown in cyan on the horizontal axis, are only observed in the distributed MaMIMO 28 GHz case, delimited around 5 μW/m^2.

C. CONFIGURATION 2: LOS VS NLOS

Figures 8a and 8b compare the reference quantities as a function of distance at 3.5 and 28 GHz, respectively. Figure 9 does so for the basic quantities. All distance profiles are highly correlated across frequency and exposure quantity. The maximum η values in LOS are highest for the reference quantities. They are lowest for the basic quantities in the

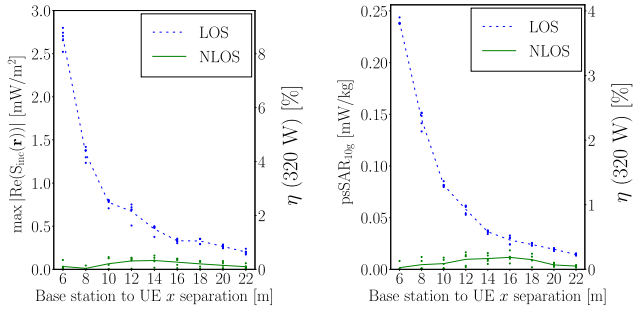

(a) For the 3.5 GHz band. (b) For the 28 GHz band.

FIGURE 8. Reference quantities normalized for a 1 W radiating BS in configuration 2. Clarification of this figure is provided in Section III-A. The exposure is closer to the limit for 3.5 GHz than for 28 GHz.

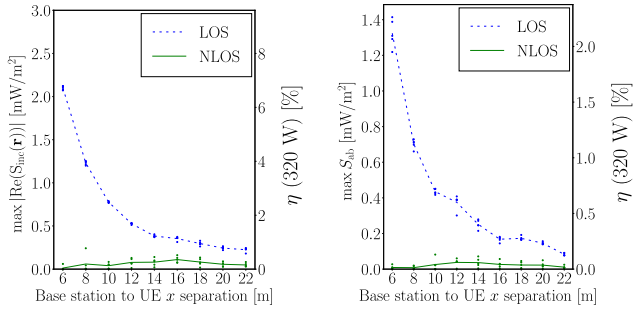

(a) For the 3.5 GHz band. (b) For the 28 GHz band.

FIGURE 9. Basic quantities normalized for a 1 W radiating BS in configuration 2. Clarification of this figure is provided in Section III-A. The exposure is closer to the limit for 3.5 GHz than for 28 GHz.

28 GHz band. Therefore we find again that the α values are lower than 1. The results for the 3.5 GHz band are similar to those found in [31]. Differences are attributed to the different configurations used. We thus find the reference levels to be conservative, guaranteeing basic quantities to be within their limits. When comparing the LOS case with the NLOS case, expected results are obtained. First, the LOS exposure quantities decrease according to a power law; the NLOS exposure quantities do not. Second, the standard deviation is lower for LOS than in the NLOS case. Both of these can be explained by the free-space LOS rays dominating the channel. The results' dependence on the environment is then lower for LOS than in the NLOS case. In the NLOS case, shadowing causes the exposure quantities to be highest 12 to 17 meters separated from the BS. This is a consequence of the NLOS blocker seen in Fig. 1b, separated 5 meters from the BS.

IV. CONCLUSION

The 5G and 6G advances in mm-Wave frequencies and distributed MaMIMO demand realistic exposure assesment. A state-of-the-art hybrid RT-FDTD tool is extended to 28 GHz by including the new absorbed power density as basic quantity set forth by the ICNIRP 2020 guidelines [18]. A multi-dimensional comparison is enabled by increasing the computational efficiency and budget. In a first configuration, clusters are observed in the distribution of exposure quantities

for distributed MaMIMO BSs. We discuss the need to normalize the exposure to the incoming power on the Rx. It is shown that exposure clusters are mainly caused by the propagation step. The highest 95th percentile among the exposure quantities expressed w.r.t. to their maximum allowed by ICNIRP is found for collocated BSs at 3.5 GHz, at 4%. With equal power, distributed BSs contribute 2 to 3 times less to all exposure metric than collocated BSs. Exposure is lower at 28 GHz compared to 3.5 GHz, due to the increased path loss. In a second configuration, the influence of UE separation and presence of a NLOS blocker is analyzed. It is found that LOS exposure follows a power law and NLOS exposure shadows the UE. In both configurations, with respect to their limits, basic quantities are 5 to 10 dB lower than reference quantities, guaranteeing ICNIRP's assumption. In future work, more comparisons with different important factors could be considered. For example, the influence of using a different precoding technique on realistic exposure with distributed MaMIMO at mm-Waves is unknown. Furthermore, the realism of industrial indoor environments could be improved. LIDAR-based models are seen as a good candidate due to their high accuracy. Lastly, the exposure of other 6G technologies such as ELAAs and holographic MaMIMO could be investigated, ideally at sub-THz frequencies.

REFERENCES

[1] G. Torfs, H. Li, S. Agneessens, J. Bauwelinck, L. Breyne, O. Caytan, W. Joseph, S. Lemey, H. Rogier, A. Thielens, and D. V. Ginste, "ATTO: Wireless networking at fiber speed," *J. Lightw. Technol.*, vol. 36, no. 8, pp. 1468–1477, Apr. 15, 2018, doi: 10.1109/JLT.2017.2783038.

[2] M Series, *Minimum Requirements Related to Technical Performance for IMT-2020 Radio Interface(s)*, document ITU-R, Rep. M.2410-0, Geneva, Switzerland, Nov. 2017.

[3] *System Architecture for the 5G System (5GS)*, ETSI and 3GPP, document 3GPP TS 23.501 v16.12.0, Sophia Antipolis, France, Mar. 2022.

[4] T. L. Marzetta, "Noncooperative cellular wireless with unlimited numbers of base station antennas," *IEEE Trans. Wireless Commun.*, vol. 9, no. 11, pp. 3590–3600, Nov. 2010, doi: 10.1109/TWC.2010.092810.091092.

[5] E. Björnson, J. Hoydis, and L. Sanguinetti, "Introduction and motivation," in *Massive MIMO Networks: Spectral, Energy, and Hardware Efficiency*. Hanover, MA, USA: Foundations and Trends in Signal Processing, 2017, ch. 1, p. 204.

[6] T. L. Marzetta, E. G. Larsson, H. Yang, and H. Q. Ngo, *Fundamentals of Massive MIMO*. Cambridge, U.K.: Cambridge Univ. Press, 2016.

[7] R. Chataut and R. Akl, "Massive MIMO systems for 5G and beyond networks—Overview, recent trends, challenges, and future research direction," *Sensors*, vol. 20, no. 10, p. 2753, May 2020, doi: 10.3390/s20102753.

[8] Search Query of Massive MIMO. *Cases*. Ericsson. Accessed: Aug. 2022. [Online]. Available: https://www.ericsson.com/en/cases?query=%22Massive%20MIMO%22

[9] E. Björnson, L. Sanguinetti, H. Wymeersch, J. Hoydis, and T. L. Marzetta, "Massive MIMO is a reality—What is next?" *Digit. Signal Process.*, vol. 94, pp. 3–20, Nov. 2019, doi: 10.1016/j.dsp.2019.06.007.

[10] X. You, D. Want, and J. Wang, *Distributed MIMO and Cell-Free Mobile Communication*, 1st ed. Singapore: Springer, 2021.

[11] H. Q. Ngo, E. G. Larsson, and T. L. Marzetta, "Aspects of favorable propagation in massive MIMO," in *Proc. 22nd Eur. Signal Process. Conf.*, 2014, pp. 76–80.

[12] A. Ashikhmin and T. Marzetta, "Pilot contamination precoding in multi-cell large scale antenna systems," in *Proc. IEEE Int. Symp. Inf. Theory Proc.*, Jul. 2012, pp. 1137–1141, doi: 10.1109/ISIT.2012.6283031.

[13] Z. Chen and E. Björnson, "Channel hardening and favorable propagation in cell-free massive MIMO with stochastic geometry," *IEEE Trans. Commun.*, vol. 66, no. 11, pp. 5205–5219, Nov. 2018, doi: 10.1109/TCOMM.2018.2846272.

[14] H. Q. Ngo, A. Ashikhmin, H. Yang, E. G. Larsson, and T. L. Marzetta, "Cell-free massive MIMO: Uniformly great service for everyone," in *Proc. IEEE 16th Int. Workshop Signal Process. Adv. Wireless Commun. (SPAWC)*, Jun. 2015, pp. 201–205, doi: 10.1109/SPAWC.2015.7227028.

[15] Nokia. *Nokia Achieves World-Record 5G Speeds*. Accessed: Aug. 2022. [Online]. Available: https://www.nokia.com/about-us/news/releases/2020/05/19/nokia-achieves-world-record-5g-speeds/

[16] Ericsson. *Ericsson Researchers Top 4.3 Gbps Downlink on 5G Millimeter Wave*. Accessed: Aug. 2022. [Online]. Available: https://Arno Thielens, Gunter Vermeeren, Emmeric Tanghe, Piet Demeester, Luc Martens, and Wout Josephwww.ericsson.com/en/news/2020/2/ericsson-achieves-record-5g-mmwave-speed

[17] *Establishing a Dialogue on Risks From Electromagnetic Fields*, World Health Org., Geneva, Switzerland, 2002.

[18] International Commission on Non-Ionizing Radiation Protection, "Guidelines for limiting exposure to electromagnetic fields (100 kHz to 300 GHz)," *Health Phys.*, vol. 118, no. 5, pp. 483–524, May 2020, doi: 10.1097/HP.0000000000001210.

[19] T. Uusitupa, I. Laakso, S. Ilvonen, and K. Nikoskinen, "SAR variation study from 300 to 5000 MHz for 15 voxel models including different postures," *Phys. Med. Biol.*, vol. 55, no. 4, p. 1157, Jan. 2010, doi: 10.1088/0031-9155/55/4/017.

[20] Y. Diao, E. A. Rashed, and A. Hirata, "Assessment of absorbed power density and temperature rise for nonplanar body model under electromagnetic exposure above 6 GHz," *Phys. Med. Biol.*, vol. 65, no. 22, Nov. 2020, Art. no. 224001, doi: 10.1088/1361-6560/abbdb7.

[21] S. Shikhantsov, A. Thielens, G. Vermeeren, E. Tanghe, P. Demeester, L. Martens, G. Torfs, and W. Joseph, "Hybrid ray-tracing/FDTD method for human exposure evaluation of a massive MIMO technology in an industrial indoor environment," *IEEE Access*, vol. 7, pp. 21020–21031, 2019, doi: 10.1109/ACCESS.2019.2897921.

[22] G. E. Athanasiadou and A. R. Nix, "Investigation into the sensitivity of the power predictions of a microcellular ray tracing propagation model," *IEEE Trans. Veh. Technol.*, vol. 49, no. 4, pp. 1140–1151, Jul. 2000, doi: 10.1109/25.875221.

[23] Y. Diao and A. Hirata, "Exposure assessment of array antennas at 28 GHz using hybrid spherical near-field transformation and FDTD method," *IEEE Trans. Electromagn. Compat.*, vol. 63, no. 5, pp. 1690–1698, Oct. 2021, doi: 10.1109/TEMC.2021.3074658.

[24] S. Shikhantsov, A. Thielens, G. Vermeeren, E. Tanghe, P. Demeester, L. Martens, and W. Joseph, "Collocated and distributed massive MIMO from the human EMF exposure perspective: A comparative study," presented at the Joint Annu. Meeting Bioelectromagnetics Soc. Eur. BioElectromagnetics Assoc., Ghent, Belgium, Oct. 2021.

[25] M. I. Iacono, E. Neufeld, E. Akinnagbe, K. Bower, J. Wolf, I. V. Oikonomidis, D. Sharma, B. Lloyd, B. J. Wilm, M. Wyss, and K. P. Pruessmann, "MIDA: A multimodal imaging-based detailed anatomical model of the human head and neck," *Public Library Sci.*, vol. 10, no. 4, pp. 1–35, Apr. 2015, doi: 10.1371/journal.pone.0124126.

[26] *MIDA Model: Ultra-High Resolution Head & Neck Model*. IT'IS Foundation. Accessed: Aug. 2022. [Online]. Available: https://itis.swiss/virtual-population/regional-human-models/mida-model/

[27] G. Vermeeren, W. Joseph, C. Olivier, and L. Martens,, "Statistic multipath exposure of a human in a realistic electromagnetic environment," *Health Phys.*, vol. 94, no. 4, pp. 345–354, Apr. 2008, doi: 10.1097/01.HP.0000298816.66888.05.

[28] R. Courant, K. Friedrichs, and H. Lewy, "Über die partiellen Differenzengleichungen der mathematischen Physik," *Math. Annalen*, vol. 100, no. 1, pp. 32–74, Dec. 1928, doi: 10.1007/BF01448839.

[29] *IEC/IEEE International Standard for Determining the Peak Spatial Average Specific Absorption Rate (SAR) in the Human Body From Wireless Communications Devices, 30 MHz—6 GHz Part 1: General Requirements for Using the Finite Difference Time Domain (FDTD) Method for SAR Calculations*, document IEEE/IEC 62704-1-2017, Oct. 2017.

[30] *IEC/IEEE International Standard—Assessment of Power Density of Human Exposure to Radio Frequency Fields From Wireless Devices in Close Proximity to the Head and Body (Frequency Range of 6 GHz to 300 GHz)—Part 2: Computational Procedure*, document IEEE/IEC 63195-2-2022, May 2022.

[31] S. Shikhantsov, A. Thielens, G. Vermeeren, P. Demeester, L. Martens, G. Torfs, and W. Joseph, "Massive MIMO propagation modeling with user-induced coupling effects using ray-tracing and FDTD," *IEEE J. Sel. Areas Commun.*, vol. 38, no. 9, pp. 1955–1963, Sep. 2020, doi: 10.1109/JSAC.2020.3000874.

ROBIN WYDAEGHE received the B.Sc. and M.Sc. degrees in engineering physics from Ghent University, Ghent, Belgium, in 2019 and 2021, respectively, where he is currently pursuing the Ph.D. degree in engineering physics. His research interests include computational electrodynamics, numerical assessment of human electromagnetic field exposure, and propagation modeling of next generation wireless networks.

SERGEI SHIKHANTSOV received the M.Sc. degree in applied physics and mathematics from the Moscow Institute of Physics and Technology (MIPT), Moscow, Russia, in 2016, and the Ph.D. degree in engineering physics from Ghent University, Ghent, Belgium, in 2022. He is currently working as a Postdoctoral Researcher with Ghent University.

EMMERIC TANGHE (Member, IEEE) was born in Tielt, Belgium, in 1982. He received the M.Sc. and Ph.D. degrees in electrical engineering from Ghent University, Ghent, Belgium, in 2005 and 2011, respectively. From 2005 to 2011, he was a Research Assistant at the Department of Information Technology, Ghent University-imec. His scientific research focused on the modeling of indoor and outdoor propagation through field measurements. In 2015, he became a Part-Time Professor in medical applications of electromagnetic fields in and around the human body. Since 2011, he has been a Postdoctoral Researcher with Ghent University-imec, where he focuses on propagation modeling. From 2012 to 2018, he was a Postdoctoral Fellow of FWO-V (Research Foundation-Flanders).

GÜNTER VERMEEREN (Member, IEEE) received the M.Sc. degree in industrial engineering from KAHO Sint-Lieven, Ghent, Belgium, in July 1998, and the M.Sc. degree in electrical engineering and the Ph.D. degree in electro-technical engineering from Ghent University, Belgium, in July 2001 and August 2013, respectively. From September 2001 to September 2002, he joined the Research and Development Department of Network Integrator Telindus, Leuven, Belgium. Since September 2002, he has been a Research Engineer with the WiCa group in the Department of Information Technology at Ghent University. His research interests include the numerical modeling as well as measurements of electromagnetic radiation in the domain of radio-frequency dosimetry, electromagnetic exposure, on-body propagation, interference in communication networks, and medical imaging systems, such as, hybrid MRI systems.

LUC MARTENS (Member, IEEE) received the M.Sc. degree in electrical engineering from Ghent University, Ghent, Belgium, in 1986, and the Ph.D. degree in 1990. From September 1986 to December 1990, he was a Research Assistant at the Department of Information Technology (INTEC), Ghent University. During this period, his scientific work focused on the physical aspects of hyperthermic cancer therapy. His research work dealt with electromagnetic and thermal modeling and the development of measurement systems for that application. Since 1991, he manages the WAVES Research Group (at the time; the Wireless and Cable Research Group), INTEC. This group is part of the IMEC Institute, since 2004. Since April 1993, he has been a Professor with Ghent University. He has authored/coauthored more than 300 publications in the domain of electromagnetic channel predictions, dosimetry, exposure systems and health, and wireless communications. His research interests include modeling and measurement of electromagnetic channels and electromagnetic exposure, e.g., around telecommunication networks and systems, such as cellular base station antennas and energy consumption of wireless networks.

PIET DEMEESTER (Fellow, IEEE) is currently a Professor with Ghent University–imec, Ghent, Belgium, where he is also the Department Director of the IDLab. He has coauthored over 1000 international publications. His research interests include distributed intelligence in the Internet of Things, machine learning and data mining, semantic intelligence, cloud and big data infrastructures, fixed networking, wireless networking, electromagnetics, and high-frequency design. He received the advanced ERC Grant.

WOUT JOSEPH (Senior Member, IEEE) was born in Ostend, Belgium, in October 1977. He received the M.Sc. and Ph.D. degrees in electrical engineering from Ghent University, Ghent, Belgium, in 2000 and 2005. From September 2000 to March 2005, he was a Research Assistant at the Department of Information Technology (INTEC), Ghent University. During this period, his scientific work focused on electromagnetic exposure assessment. Since April 2005, he has been a Postdoctoral Researcher with imec-UGent/INTEC. From October 2007 to October 2013, he was a Postdoctoral Fellow of FWO-V (Research Foundation-Flanders). Since October 2009, he has been a Professor in the domain of experimental characterization of wireless communication systems. His research interests include measuring and modeling electromagnetic fields around base stations for mobile communications, health effects of exposure to electromagnetic radiation, electromagnetic exposure assessment, propagation for wireless communication systems, and antennas and calibration. Furthermore, he specializes in wireless performance analysis and quality of experience.